Simulation study of nonergodicity transitions: Gelation in colloidal systems with short-range attractions

Antonio M. Puertas
Department of Physics, University of Almeria, 04120 Almeria, Spain

Matthias Fuchs
Institut Charles Sadron, 67083 Strasbourg Cedex, France

Michael E. Cates
School of Physics, University of Edinburgh, JCMB Kings Buildings, Edinburgh EH9 3JZ, United Kingdom

(Received 31 October 2002; published 26 March 2003)

Computer simulations were used to study the gel transition occurring in colloidal systems with short-range attractions. A colloid-polymer mixture was modeled and the results were compared with mode coupling theory (MCT) expectations and with the results for other systems (hard-spheres system and Lennard-Jones system). The self-intermediate scattering function and the mean squared displacement were used as the main dynamical quantities. Two different colloid packing fractions have been studied. For the lower packing fraction, α-scaling holds and the wave-vector analysis of the correlation function shows that gelation is a regular nonergodicity transition within MCT. The leading mechanism for the novel nonergodicity transition is identified as the bond formation caused by the short-range attraction. The time scale and diffusion coefficient also show qualitatively the expected behavior, although different exponents are found for the power-law divergences of these two quantities. The non-Gaussian parameter was also studied and a very large correction to Gaussian behavior was found. The system with higher colloid packing fraction shows indications of a nearby high-order singularity, causing α scaling to fail, but the general expectations for nonergodicity transitions still hold.

DOI: 10.1103/PhysRevE.67.031406 PACS number(s): 82.70.Dd, 64.70.Pf, 82.70.Gg

I. INTRODUCTION

Colloidal suspensions are often referred to as model systems for studying fundamental problems in condensed matter physics [1]. Most of the properties of colloidal systems are similar to those of simple liquids, except for the difference in the time scales involved in the processes in liquids or colloids, making the latter more useful in the study of some basic questions. Moreover, the interaction forces between particles in a colloidal system are easily tailored (e.g., by adding salt or polymer). However, there are some features found only in colloids, such as aggregation or gelation, which makes the study of these systems even more fascinating.

Gel formation, or gelation, is seen in systems with strong short-range attractions, and is a universal phenomenon observed experimentally in many different systems, ranging from colloid-polymer mixtures [2,3] to charged systems [4], or to globular protein systems [5]. Gelation is the formation of a percolating network (typically fractal) of dense and more dilute regions of particles with voids that coarsen up to a certain size and freeze when the gel is formed. This process is observed in the structure factor as a low-q scattering peak that moves to lower q, increasing its height, and then arrests [6–8]. Description of this phenomenon has been attempted with percolation theories, theories of phase separation for states inside the liquid-gas binodal (which is metastable with respect to fluid-solid coexistence for short interaction ranges) or in terms of a glass transition of a cluster of particles [8,9].

Recently, acknowledging its nonequilibrium character, gelation has been interpreted using the formalism of mode coupling theory (MCT) for nonergodicity transitions [10–12]. This approach views the gel as particles trapped by a network of bonds which hinders the particle motion, resulting in a nonergodic state. Thus, gelation is caused by formation of long lived bonds, whose collective arrest is described as a normal nonergodicity transition. (This is distinct from many earlier approaches whereby the bonds were assumed to form irreversibly from the outset.) In the present simulation study we want to test this suggestion critically, thereby establishing the existence or otherwise of a nonergodicity transition corresponding to bonding network formation.

Also present in colloidal systems is the equivalent of the usual glass transition in simple liquids, which occurs at high densities, and is driven by steric imprisonment. This transition has been studied experimentally and compared to MCT thoroughly [13–16]. When two different nonergodicity transitions are observed in a system, MCT predicts a high-order singularity in the region where the driving mechanisms for both transitions are present [17–19]. Therefore, a higher-order transition is expected at high attraction strength and high density in colloidal systems with attractive interactions [10,20,21].

Computer simulations have been used to test the expectations from the MCT in many different systems, such as a Lennard-Jones liquid [22–25], water [26,27], polymers [28–31] and strong glass formers [32–34]. The tests have shown that the predictions from the MCT are correct, not only qualitatively but also, in part, quantitatively [33,35]. However, these have also pointed out some differences, especially in the spatial correlations of particle mobility [36–39]. In none of these simulated systems, however, did gelation oc-

cur, presumably because the attractions were not short ranged enough.

In this work we have used molecular dynamics simulations to study the properties of the gel transition, and compared them with the predictions from the MCT. (This was initiated in Ref. [40] where some further results may be found.) We take the numerous universal predictions of the theory to test the scenario qualitatively. Comparing with quantitative predictions available for systems of hard spheres [41,42], spheres with short-range attractions [10–12,21], and the mentioned simulation studies, we identify the mechanism driving the nonergodicity transition, which is the cause of gelation for moderately dense suspensions. Molecular dynamics were used instead of Brownian dynamics because the choice of microscopic dynamics does not affect the relaxational dynamics of a system close to a nonergodicity transition [24]. By means of the Asakura-Oosawa interaction potential [43], we simulate the behavior of a colloid-polymer mixture, which is a well-understood system [44–47]. For short interaction ranges, this system exhibits a fluid-crystal transition, at intermediate densities and increasing attraction strength, with a liquid-gas transition metastable to the fluid-crystal one. In our simulations, the system was modified to prevent both of these phase transitions from occurring, in order to be able to study the transition from the fluid to the nonequilibrium states. Another detailed analysis of the driving mechanisms for gels and glasses has been performed in Ref. [48], where a system of square well particles was simulated and isotherm and isodiffusivity lines were studied.

This paper is organized as follows: Section II describes some results from MCT which will be used in the subsequent analysis of the simulation results. In Sec. III the simulation method is presented and the details are given. Section IV deals with the results and is divided into four subsections studying (i) the correlation function, (ii) the time scale and the diffusion coefficient, (iii) the mean squared displacement, and (iv) a higher colloid concentration. Finally, in Sec. V we present the conclusions of this work.

II. MODE COUPLING THEORY

In this section we will present the most important MCT results on nonergodicity transitions. MCT attempts a description of the density correlator and its self-part, in terms of a fluctuating-force correlator [49,50]. In this paper, only the self-part of the density correlator will be studied, which is defined as

$$\Phi_q^s(t)=\langle \exp\{i\mathbf{q}[\mathbf{r}_j(t)-\mathbf{r}_j(0)]\}\rangle, \tag{1}$$

where the brackets denote average over particle j and time origin, and $\mathbf{q}$ is the wave vector. The equation of motion of Φ_q^s in Brownian (coarse grained) dynamics is given by

$$\tau_q \partial_t \Phi_q^s(t)+\Phi_q^s(t)+\int_0^t m_q(t-t')\partial_{t'}\Phi_q^s(t')dt'=0, \tag{2}$$

where τ_q is a single-particle diffusive time scale and $m_q(t)$ is a mode coupling kernel that describes the cage effect [51]. Within MCT, glass states are given by nonzero solutions of this equation for the long-time limit of $\Phi_q^s(t\to\infty)=f_q^s$, the so-called *nonergodicity parameter*. It describes the glass structure and may also be called *Lamb-Mössbauer factor*. The glass transition is marked by a (generally) discontinuous transition from the unique trivial solution in the liquid, $f_q^s=0$, to multiple solutions in the glass, $f_q^s>0$, where only the highest solution is physical. Glass transitions can be classified according to the number $l-1$ of nontrivial solutions merging with the highest one, and the type of transition is noted as A_l.

For liquid states close to the glass, a two-step decay is observed for the correlator; the plateau is at f_q^s and signals the proximity of the glass transition. Around this plateau, Φ_q^s shows some universal properties, depending on the type of transition. For the most common type of transition A_2, the decay to the plateau and that from the plateau, can both be expressed as power-law expansions. In particular, the decay from the plateau is given by

$$\Phi_q^s(t)=f_q^s-h_q^{(1)}(t/\tau)^b+h_q^{(2)}(t/\tau)^{2b}+O((t/\tau)^{3b}) \tag{3}$$

with $h_q^{(1)}$ and $h_q^{(2)}$ being amplitudes and τ being the final or α-relaxation time scale. b is known as the von Schweidler exponent, which depends on the details of the interaction potential. Expression (3) implies time scaling for the decay from the plateau, called α decay, for different states close to the glass transition. The time scale τ diverges as the glass transition is approached according to a power law, with an exponent γ, which can be related to the von Schweidler exponent: $\tau\sim|\sigma|^{-\gamma}$, with σ being the distance to the transition [49,50]. On the other hand, the wave-vector dependence of the nonergodicity parameter and amplitudes gives some nonuniversal properties of the transition, providing information about the mechanism causing the nonergodicity transition.

For high-order singularities, the fluid states close by show again a two-step decay in the correlation function, but the decays to and from the plateau are no longer power-law expansions. Instead, logarithmic laws are obtained [18,19]. A salient feature is that a logarithmic decay around the plateau is predicted:

$$\Phi_q^s(t)=f_q^{sA}-C_q\ln(t/t_1), \tag{4}$$

where f_q^{sA} is the nonergodicity parameter of the high order singularity, C_q is an amplitude and t_1 is a time scale (the time when the correlator lies on the plateau).

The mean squared displacement (MSD) can be studied instead of the correlation function, obtaining a similar two-step behavior. Similar asymptotic laws to describe the decay to and from the plateau can be derived, and the parameters and exponents can be related to those of the correlation function [42]. The value of the plateau in the MSD defines the *localization length* and is a measure of the size of the cage. However, it should be noticed that the cage, as formed by other particles, is constantly restructuring cooperatively. Only when the particles have broken free of their cages, diffusive motion is observed, with a self-diffusion coefficient

D_s that tends to zero as the glass transition is approached as $D_s \sim |\sigma|^{\gamma}$ for the usual A_2 transitions.

Two different nonergodicity transitions have been found in colloidal systems with a short-range attraction [10,21]: a steric hindrance driven glass transition and an attraction driven gel transition [10–12]. While the first is found at high densities and is qualitatively similar to the glass transition in the hard-sphere system (HSS) or Lennard-Jones system (LJS), the gel transition occurs at high attraction strength for all volume fractions. Different properties for these two transitions are predicted, the main difference arising from the driving mechanism: the localization length is shorter in the gel than in the glass, resulting in higher nonergodicity parameters. Also, a smaller von Schweidler exponent for the gel than for the glass is expected, implying a higher value of γ, i.e., the transition as observed by τ_q or D_s is more abrupt.

The actual shape of the nonergodicity transition line depends on the details of the interaction potential, although some general features can be found. From lower to higher interaction strength, the glass line is slanted to higher concentrations, showing that a weak attraction *fluidizes* the glass. However, at even higher interaction strengths, the gel transition occurs at a lower colloid density the higher the attraction strength. As a result, a reentrance transition is obtained at high colloid volume fractions. The line may be wedge shaped or curved in this region, depending on the range of the interaction. If the line is wedge shaped, a high-order transition (generically A_3) is present near the corner, whereas none exists if the line is smoothly continuous. An A_4 singularity appears right at the vanishing of the A_3 point when the line first becomes smooth [21].

III. SIMULATION DETAILS

Equilibrium molecular dynamics simulations mimicking a colloid-polymer mixture were performed for a system composed of 1000 soft-core polydisperse colloidal particles. The core-core interaction between particles was modeled by

$$V_{sc}(r) = k_B T \left(\frac{r}{a_{12}} \right)^{-36}, \tag{5}$$

where $a_{12} = a_1 + a_2$, with a_1 and a_2 being the radii of the interacting particles. A flat distribution of radii with a width of $\delta = 0.1a$, where a is the mean radius, was used. The exponent in V_{sc} was selected high enough to avoid problems related to the softness of the potential [52]. The polymer induces an attractive depletion interaction between the colloidal particles, which was modeled by the Asakura-Oosawa interaction potential [43,47]. The extension of this potential to take polydispersity into account reads [53]

$$V_{AO}(r) = -k_B T \phi_p \left\{ \left[(\overline{\eta}+1)^3 - \frac{3r}{4\xi}(\overline{\eta}+1)^2 + \frac{r^3}{16\xi^3} \right] + \frac{3\xi}{4r}(\eta_1 - \eta_2)^2 \left[(\overline{\eta}+1) - \frac{r}{2\xi} \right]^2 \right\} \tag{6}$$

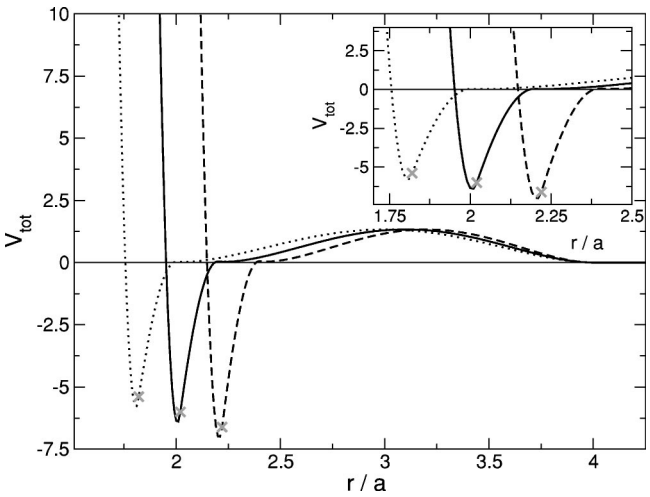

FIG. 1. Total pair interaction potential $V_{\rm tot}$ as a function of the radial distance $r = |\mathbf{r}_1 - \mathbf{r}_2|$ for three different particle pairs; a pair of particles with minimal radii $a_1 = a_2 = a - \delta$, one with average radii $a_1 = a_2 = a$, and one with maximal $a_1 = a_2 = a + \delta$ (from left to right). The inset shows the enlarged region of the attractive minimum. Crosses mark where the parabolic minimum smoothly matches Eq. (6).

for $r \leqslant 2(a_{12} + \xi)$ and 0 for larger distances. Here, $\eta_i = a_i / \xi$; $\overline{\eta} = (\eta_1 + \eta_2)/2$, and ϕ_p is the volume fraction of the polymer. Note that the range of the potential is given by the polymer size ξ and its strength is given by ϕ_p. This potential was modified around $r = a_{12}$ to ensure that the minimum of the total potential $(V_{sc} + V_{A0})$ occurs at this point: for $r \leqslant 2a_{12} + \xi/5$ a parabolic form that connects analytically to V_{AO} at $2a_{12} + \xi/5$ and has a minimum in $2a_{12}$ was used. In our simulations, the range of the interaction 2ξ was set to $0.2a$, which would correspond to polymers with $R_g/a = 0.1$ where R_g is the radius of gyration.

A long-range repulsive barrier was added to the interaction potential in order to prevent liquid-gas separation (as shown below). The barrier had a maximal height of $1 k_B T$ according to a fourth-order polynomial

$$V_{bar}(r) = k_B T \left\{ \left(\frac{r - r_1}{r_0 - r_1} \right)^4 - 2 \left(\frac{r - r_1}{r_0 - r_1} \right)^2 + 1 \right\} \tag{7}$$

for $r_0 \leqslant r \leqslant r_1$ and zero otherwise. The limits of the barrier were set to $r_0 = 2(a_{12} + \xi)$ and $r_1 = 4a$, which was enough to prevent phase separation. The maximum height of the barrier equals the depth of the depletion interaction at contact for $\phi_p = 0.0625$, much lower than the values where the gel transition takes place. The resulting total interaction potential $V_{tot} = V_{sc} + V_{AO} + V_{bar}$ is analytical everywhere. It is shown in Fig. 1, where, in order to indicate the spread induced by polydispersity, the potentials among three different pairs with differing radii are plotted.

In our simulations, lengths were measured in units of the mean radius a and time in units of $\sqrt{4a^2/3v^2}$, where the thermal velocity v was set to $\sqrt{4/3}$. Equations of motion were integrated using the velocity-Verlet algorithm, in the canonical ensemble (constant *NTV*), to mimick the colloidal

dynamics. Every n_t time steps, the velocity of the particles was rescaled to ensure constant temperature. No effect of n_t was observed for well equilibrated samples. The time step was set to 0.0025. Equilibration of the systems was tested by monitoring the total energy, and other order parameters (see below), and by measuring $\Phi_q^s(t)$ and the MSD at different initial times. When the order parameters were constant and the $\Phi_q^s(t)$ and MSD curves showed no dependence on the initial time (ageing), the system was considered to be equilibrated.

The volume fraction of the colloidal particles, $\phi_c = \frac{4}{3}\pi a^3[1+(\delta/a)^2]n_c$, with n_c being the colloid number density, and the polymer volume fraction ϕ_p were the control parameters used to identify the states in the phase diagram.

In order to explore the whole $\phi_p - \phi_c$ plane in search of the gel transition, phase transitions that forbid access (in equilibrium) to important parts of the plane must be prevented. Several order parameters were used to identify different kinds of ordering in our system and to monitor whether unwanted liquid-gas or fluid-crystal transitions were taking place. First, the onset of phase separation involving states of different density can be detected by dividing the system into n^3 boxes and measuring the density in every box. The ''demixing'' order parameter is defined as the standard deviation of the distribution of densities:

$$\Psi_n = \sum_{k=0}^{n^3} (\rho_k - \overline{\rho})^2, \tag{8}$$

where ρ_k is the density of particles in box k and $\overline{\rho}$ is the mean density. This parameter is close to zero for an homogeneous system and increases if it demixes into phases of different density. In our case, n has been set to 4, implying 64 boxes, and a box edge of about $5a$ (depending on ϕ_c). On the other hand, the orientational order parameter Q_6, as defined by Steinhardt and co-workers [54,55], signals the presence of an ordered phase and is used to detect crystallization.

The phase diagram was probed using these parameters. In Fig. 2 the results are presented for a bare system (monodisperse and without the long-range barrier), a polydisperse system without the long-range barrier, and the final system with both polydispersity and barrier. In this figure, the colloid volume fraction is constant, $\phi_c = 0.40$, and the polymer concentration varies; an isochore is studied. The sudden increase in both Ψ_4 and Q_6 occurring at $\phi_p = 0.20$ for the bare system signals the crystallization boundary, in accordance with Dijkstra *et al.* [47]. Because of the short range of the potential, this system has no liquid phase, i.e., the liquid-gas coexistence is metastable with respect to the crystal-gas transition.

When polydispersity is introduced in the system, crystallization is prevented, as indicated by the constant trend of both parameters close to $\phi_p = 0.20$. However, as the system now does not crystallize, the liquid-gas transition can be reached upon increasing the strength of the interaction. This demixing is signaled by an increase in Ψ_4, not involving local ordering. In order to avoid this separation, a long-range barrier has been introduced in the interaction potential. The

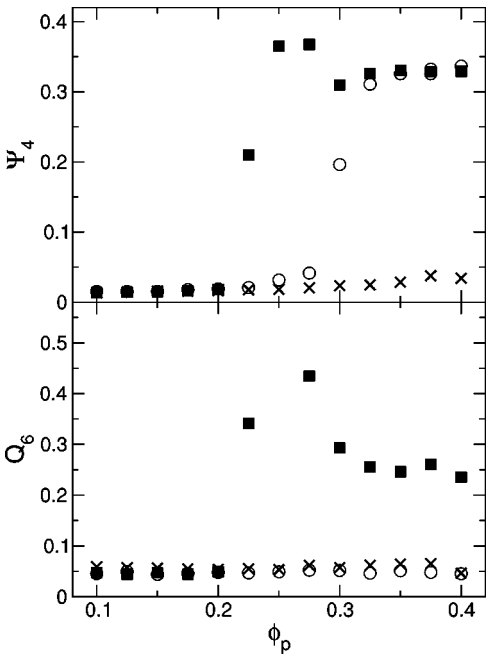

FIG. 2. Demixing (Ψ_4) and orientational (Q_6) parameters for $\phi_c = 0.40$ and increasing polymer fraction ϕ_p for different systems: monodisperse without long-range barrier (squares), polydisperse without barrier (circles), and polydisperse with long-range barrier (crosses).

energy of a dense phase is raised, and demixing is thus energetically unfavorable. Figure 2 shows that liquid-gas separation is indeed inhibited by the repulsive barrier. Instead, individual voids of finite size are created in the system, causing a low-q peak in the structure factor $S(q)$ presented in Fig. 3. There, $S(q)$ is shown for different polymer fractions, ranging from no attraction ($\phi_p = 0$) to the closest state to the gel we have accessed ($\phi_p = 0.425$).

In the inset to Fig. 3, the pair distribution function, $g(r)$,

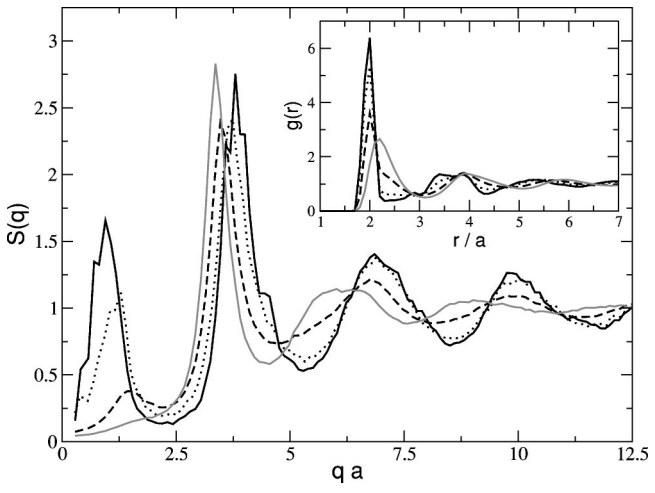

FIG. 3. Structure factors for different polymer fractions at $\phi_c = 0.40$: $\phi_p = 0$ gray line, $\phi_p = 0.2$ dashed line, $\phi_p = 0.35$ dotted line, and $\phi_p = 0.425$ solid black line. Note the low-q peak rise as ϕ_p is increased. Inset: Pair distribution function $g(r)$ for the same states.

is presented for the same states as the structure factor. The value at contact, $r=2$, increases continuously as the attraction strength grows, signaling increased local contact probabilities. This process will be shown to be responsible for the gel transition. In S_q it becomes evident as an increase in the oscillations for large q.

The low-q peak in the structure factor resembles the low-angle peak observed in light scattering experiments with colloidal gels [6,8]. However, whereas the peak in our system is an equilibrium property, induced by the specific shape of the interaction potential, the experimental peak has a nonequilibrium origin. We also checked for the possibility of microphase separation, which in some cases can be induced by a repulsive barrier [56]. In our case, the small angle peak continuously increases with ϕ_p, but stays finite and smaller than the neighboring peak as we approach the gel transition. We interpret this to indicate that we do not have microphase separation, and we also observed no other signs of such ordering. Furthermore, since the relevant wave vectors in the MCT calculation of the gel transition are the high ones (around $2\pi/\xi$), the change in the low-q region in the structure factor is expected to have little effect on the gel transition.

IV. RESULTS AND DISCUSSION

This system has been previously shown to undergo both the glass and gel transitions as stated by MCT. It also exhibits a logarithmic decay in the correlation function at high colloid and polymer concentrations, indicating a high-order singularity in that region [40]. In this section we will discuss the properties of the gel transition, and compare them with MCT and with those of the HSS and other systems, which are similar to the glass transition at high colloid concentrations. We test for differences by comparing quantitatively the nonuniversal features of the transition, which will aid in the identification of the driving mechanism.

The gel line is predicted to extend to low packing fractions with the same qualitative properties. In order to test these properties, we have performed simulations at two different colloid concentrations, $\phi_c=0.40$ and $\phi_c=0.50$, where the gel line is far away from the percolation one. At high concentration, the higher-order singularity is expected to affect the equilibrium states, disturbing some features of the gel transition.

A. Self-intermediate scattering function

The scaling prediction for the α-decay of states close to a nonergodicity transition is tested in Fig. 4 for constant colloid packing fraction $\phi_c=0.40$. Two different representative wave vectors are presented in this figure, $q=6.9$ and $q=15$. As observed at the glass transition in the HSS and many other different systems [22,23,27,31,34,40], the α-scaling property holds. In comparing these correlation functions with those typical for the HSS or LJS, it is noticed that in Fig. 4 the α decay of the correlators is more stretched, implying a smaller von Schweidler exponent at the gel transition than at the glass transition. Because of this stretching

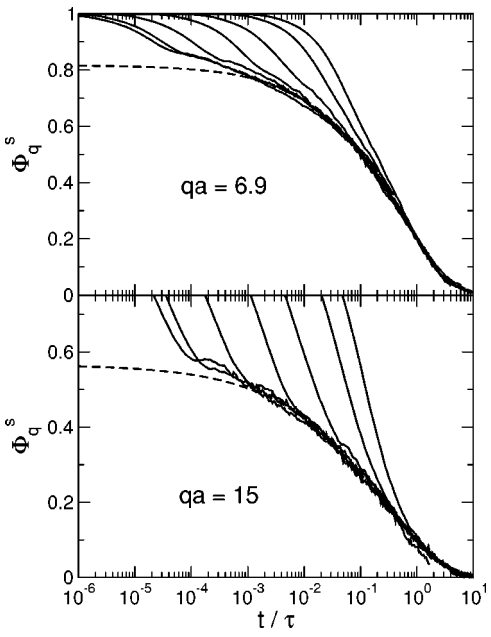

FIG. 4. Intermediate scattering function (self-part) Φ_q^s vs rescaled time with the α-time scale τ_q for different states: $\phi_c=0.40$ and $\phi_p=0.375,0.39,0.40,0.41,0.415,0.42,0.425$ from right to left. Two different wave vectors are studied: $q=6.9$ (upper panel) and $q=15$ (lower panel), with the KWW fits (dashed line) included.

in the α decay, a clear plateau is not observed, although a slowing down of more than four decades is studied. Nevertheless, extrapolating the relaxation curves to extract plateau values, much higher values are found than at the glass transition in the HSS or the LJS. The same problem with the plateau was reported in Ref. [48]. The nonergodicity parameters were obtained from Kohlrausch fittings in that case.

We have analyzed the state $\phi_c=0.40$ and $\phi_p=0.42$ in more detail, which shows four decades of slowing down compared to the purely repulsive situation upon turning on the attraction. Because scaling is observed in Fig. 4, studying only one state is enough to analyze the α decay of the correlation function. The slowest state $\phi_p=0.425$ was not chosen because it strongly deviates from the expected behavior of τ_q vs ϕ_p (see Fig. 8 and discussion thereafter). The correlation functions at different wave vectors for state $\phi_c=0.40$ and $\phi_p=0.42$ are presented in Fig. 5. The range of wave vectors studied, where the plateau height changes, is much wider than the range for a similar change in f_q at the glass transition of hard spheres or Lennard-Jones particles. This feature indicates that the relevant distances for the gel transition are much shorter than for the usual glass transition [40,48].

The correlation functions were measured until the average particle displacement was $5a$, which is one-fourth of the box size $(21.95a)$. Thus, extending this measurement to longer times in order to observe the whole α decay at low q is troublesome. If the diffusion coefficient diverges at the same rate as the α-time scale (as predicted by MCT), this problem would not appear. Thus, we are also observing a discrepancy between both time scale divergences, which will be further discussed below.

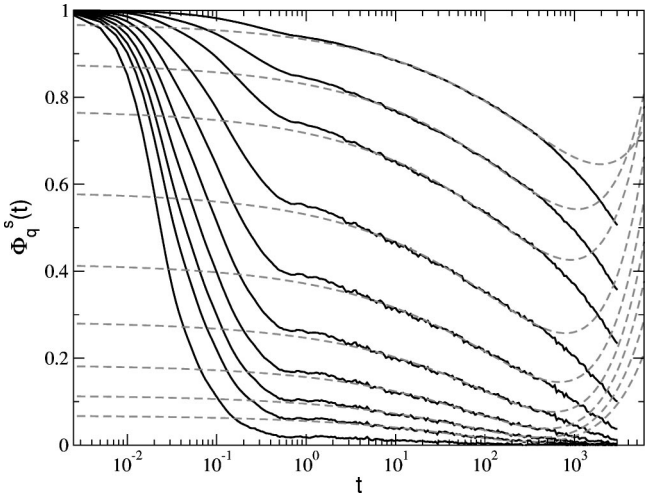

FIG. 5. Intermediate scattering function (self-part) Φ_q^s for the state $\phi_c = 0.40$ and $\phi_p = 0.42$, for different wave vectors (from top to bottom): $q = 3.9, 6.9, 9.9, 15, 20, 25, 30, 35, 40, 50$. The dashed lines are fittings from Eq. (3) up to second order, with the same von Schweidler exponent for all q.

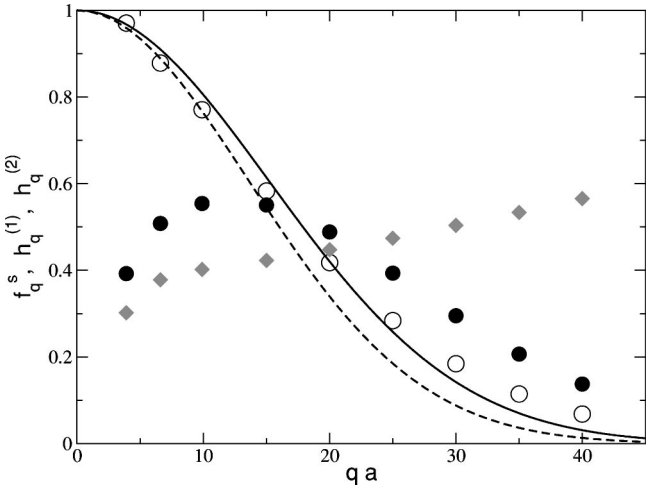

FIG. 6. Nonergodicity parameter f_q^s (open circles) and first- (filled circles) and second-order (diamonds) amplitudes from the fittings in Fig. 5 with $b = 0.37$ for all wave vectors. The lines give the Gaussian approximation from Eq. (9) fitted to all wave vectors (solid line) and the three lowest wave vectors (dashed line).

The impossibility of observing a clear plateau, as mentioned above, makes it more difficult to analyze the correlators, since f_q^s cannot be fixed *a priori*. Therefore, the α decay of the correlation functions has been fitted using expression (3), with f_q^s, $h_q^{(1)}$ and $h_q^{(2)}$ as fitting parameters. The von Schweidler exponent was also fitted but was kept identical for different wave vectors. It was found as $b = 0.37$, and the other results for the fitting parameters are shown in Fig. 6. The trends of these parameters are similar to that of the glass transitions in both HSS and LJS, but over a wider q range in the gel case. This indicates that the localization length is quite different in the present system. The nonergodicity parameter exhibits a bell shaped curve, whereas the first-order amplitude describes a maximum. The latter is determined from the fit up to a prefactor that depends on the choice of τ in Eq. (3). As an estimate, we have used τ_q for $q = 9.9$ [τ_q is defined by $\Phi_q^s(\tau_q) = f_q/e$], which yields values that are similar (in magnitude) to the HSS. The second amplitude shows a monotonically increasing behavior with q, in accordance with the HSS, but it is always positive, unlike the HSS where it goes through zero at the peak of $h_q^{(1)}$.

The nonergodicity parameter f_q^s can be approximated using the Gaussian expression

$$f_q^s \approx \exp\{-q^2 r_l^2/6\}, \tag{9}$$

where r_l is the localization length. This approximation is known to be valid for low wave vectors, and important deviations from the Gaussian behavior are expected close to the glass transition. However, the value for the localization length obtained from fitting this curve (solid line in Fig. 6) can be used as an estimate of that in the MSD.

The localization length so obtained is $r_l^2 = 0.0126a^2$, which is much smaller than for the HSS or the LJS, where r_l is of the order of the Lindemann distance. This feature shows that the process causing the nonergodic transition in our case has a typical distance much smaller than in the case of glass transitions in the HSS or the LJS. This agrees with the observation and discussion about the height of the plateaus, and of the different q range covered by f_q^s in Fig. 6. Whereas the glass transition in the HSS is driven by core-core repulsions, the gel transition is caused by the short-range attraction, therefore by *bonds* between particles (see inset to Fig. 3) whose size is of the order of the interaction range. An interesting analogy has been established between the mechanisms driving the formation of gels and glasses and the freezing transition [57].

The α decay of near-nonergodic states can be also studied using the Kohlrausch-Williams-Watts (KWW) stretched exponential. The KWW expression is given by

$$\Phi_q^K(t) = A_q \exp\left\{-\left(\frac{t}{\tau_q^K}\right)^{\beta_q}\right\}, \tag{10}$$

where β_q is known as Kohlrausch exponent, which has been shown to coincide with the von Schweidler exponent at high wave vectors [58]. This expression has been fitted to very different systems, and describes the α decay down to zero. We have fitted this expression to the α decay in our system. However, since the correlators in Fig. 5 do not show the complete α decay, we have fitted expression (10) to the master curve, obtained from the α rescaling. Two of these fittings are presented in Fig. 4 by the dashed lines, showing that the KWW stretched exponential describes well the α decay in this system.

The fitting parameters A_q, β_q, and τ_q, are presented in Fig. 7 and are compared with the corresponding parameters in the von Schweidler formalism. In such a way, A_q is compared with the nonergodicity parameter, β_q is compared with the von Schweidler exponent, and the τ_q^K is compared with τ_q. As expected, the height of the plateau can be determined equally well both by the KWW or von Schweidler analysis.

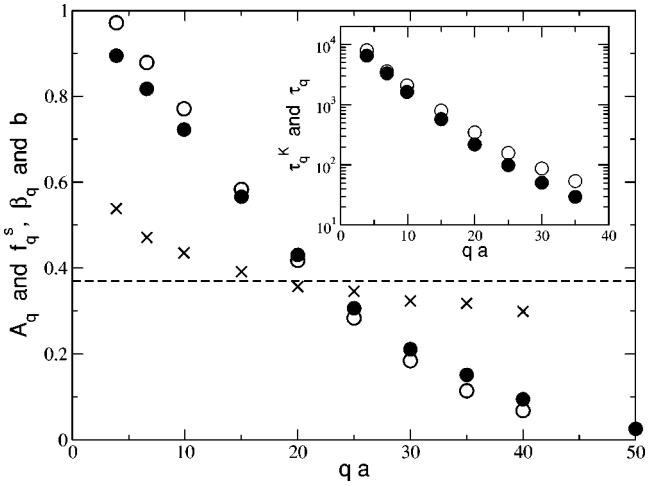

FIG. 7. Parameters used in the KWW fittings and comparison with the von Schweidler fitting. Main figure: A_q (closed circles) and f_q^s (open circles), β_q (crosses), and b (horizontal dashed line). Inset: τ_q^K (closed circles) and τ_q (open circles).

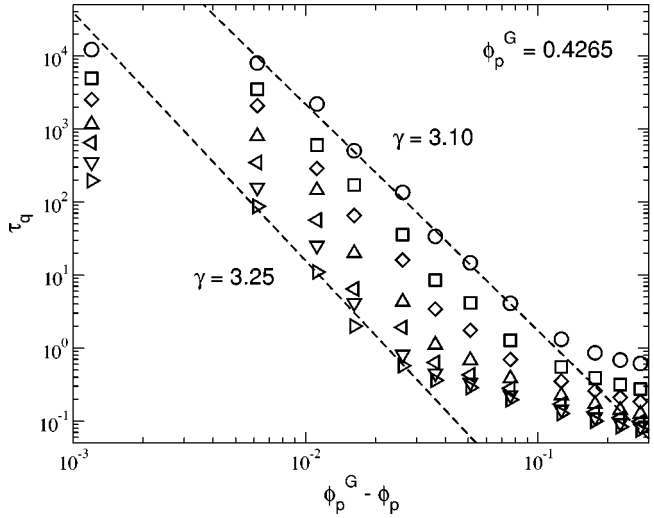

FIG. 8. Wave-vector-dependent time scale τ_q vs $\phi_p^G - \phi_p$ for the isochore $\phi_c = 0.40$ for different wave vectors; symbols from top to bottom correspond to $q = 3.9, 6.9, 9.9, 15, 20, 25, 30$. The lines are power-law fittings to $q = 3.9$ and $q = 30$. In all cases γ keeps close to these two values.

The same holds for the time scales τ_q^{KWW} and τ_q. The Kohlraush exponent is expected to tend to 1 at low wave vectors, and to the value of the von Schweidler exponent at high q. The low-q limit is explained because diffusion is the dominant process over long distances, whereas at short distances (comparable to the cage size) the dynamics is dominated by the cooperative local rearrangements. This behavior is predicted from MCT [58], and has been observed in different systems, such as molecular glass formers [59], and in simulations of polymer melts [31] and of water [60]. In our case, the low-q limit is not observed, but β rises as the wave vector decreases, indicating that the expected behavior may appear at a lower q below the small angle peak in $S(q)$. At a high wave vector, the Kohlraush exponent crosses the von Schweidler value, but stays close to it. Although an exact agreement is not observed, we may conclude that the correct general trend is obtained.

B. Time scale and diffusion coefficient

An important universal prediction of MCT is the existence of power-law divergences for both the time scale τ and the inverse of the self-diffusion coefficient D_s, with the same exponent in both cases, γ:

$$\tau_q \sim (\phi_p^G - \phi_p)^{-\gamma} \text{ and } D_s \sim (\phi_p^G - \phi_p)^{\gamma}, \qquad (11)$$

where ϕ_p^G is the polymer volume fraction where the gel transition occurs. The relation between exponent γ and the von Schweidler exponent b is also universally established by MCT [50].

Testing of the power-law divergence (and measuring of γ) is usually carried out plotting τ_q as a function of $\phi_p^G - \phi_p$ for different values of ϕ_p^G, looking for a straight line. This method is cumbersome, even more as deviations from it are expected for states close to the transition, and precise values for γ and ϕ_p^G cannot be given. To avoid this difficulty, we have calculated γ from b, as given by MCT, and with this particular value of the exponent looked for the power-law divergence. In such a way, we are testing the *compatibility* of the MCT predictions with our data.

Figure 8 shows the wave-vector-dependent time scale τ_q vs $\phi_p^G - \phi_p$ for different wave vectors. For every wave vector, $\tau_q^{1/\gamma}$ was extrapolated to zero, yielding a value for the polymer fraction at the gel transition, $\phi_p^{G,q}$. The final value of ϕ_p^G, used in Fig. 8, was calculated as the average value for all wave vectors studied. The linear trends in Fig. 8 for $\phi_p^G - \phi_p > 5 \times 10^{-3}$ show the power-law behavior predicted by MCT, with exponents $\gamma = 3.1$ and $\phi_p^G = 0.4265$. The closest state to the gel transition $\phi_p = 0.425$ deviates from the power-law behavior observed for lower polymer fractions. Similar deviations have been observed in the HSS and LJS and can tentatively be attributed to thermally activated processes (or hopping events) [61].

As shown in Eq. (11), MCT predicts a power law for the self-diffusion coefficient D_s with the same exponent as the divergence of the time scale. Simulations on HSS and LJS have shown that a power-law divergence is indeed obtained, but with a different exponent than in the case of τ_q. Using the same procedure as described above (calculating γ from b and extrapolating $D_s^{-1/\gamma}$ to obtain ϕ_p^G) yields $\phi_p^G = 0.4519$, with the same γ as for the time scale. This value of ϕ_p^G is too far from that obtained using τ_q. Therefore, we cannot have similar ϕ_p^G and γ to explain the behavior of both τ_q and D_s, implying that the MCT prediction, Eq. (11), is violated.

In Fig. 9, we present D_s vs $\phi_p^G - \phi_p$ using for ϕ_p^G both the value estimated from τ_q and that from D_s. We consider more desirable to have similar ϕ_p^G to explain the behavior of τ_q and D_s, even though this implies two different γ: $\gamma = 3.1$ for τ_q and $\gamma = 1.23$ for D_s. As obtained in other nonergodicity transitions [22,31,34], the γ exponent is lower in the diffusion coefficient than in the time scale, although the difference between both values of γ is bigger in our case.

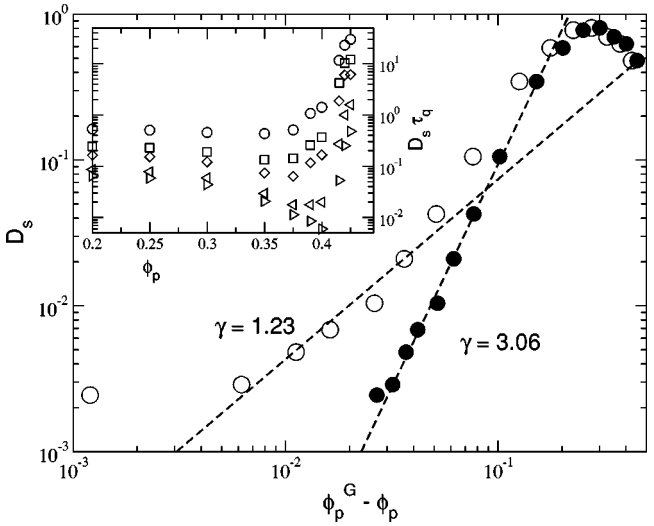

FIG. 9. Self-diffusion coefficient D_s vs $\phi_p^G - \phi_p$ for two values of ϕ_p^G: $\phi_p^G = 0.4519$ (closed circles) and $\phi_p^G = 0.4265$ (open circles). The dashed lines are the power-law fittings to the data, with the exponent shown in the figure. Inset: $D_s\tau_q$ vs polymer fraction for different wave vectors. Symbols as in Fig. 8.

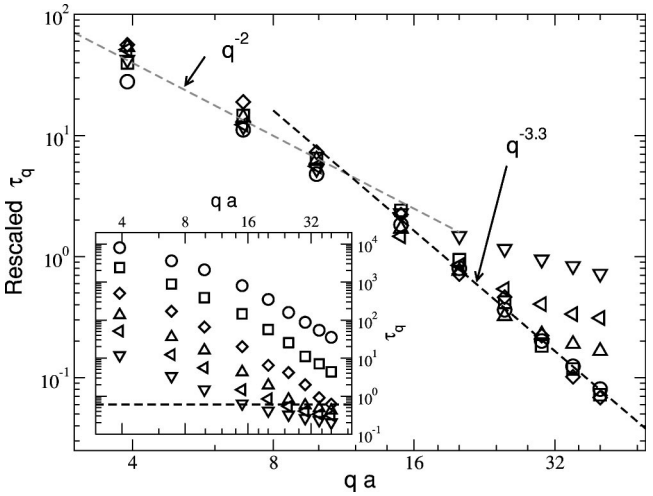

FIG. 10. (Inset) Time scale τ_q as a function of the wave vector q for different states close to the gel: $\phi_p = 0.42$ (circles), $\phi_p = 0.415$ (squares), $\phi_p = 0.41$ (diamonds), $\phi_p = 0.40$ (upward triangles), $\phi_p = 0.39$ (left-ward triangles), and $\phi_p = 0.375$ (downward triangles). Main body: same data, rescaled to collapse in the low-q power-law behavior. The dashed lines show power-law behaviors with exponents 2 (gray line) and 3.3 (black line).

In order to stress the different γ exponents in the divergence of the time scale and $1/D_s$, we have plotted $D_s\tau_q$ as a function of ϕ_p for different wave vectors in the inset to Fig. 9. This product, which should be constant according to MCT, diverges as the polymer fraction approaches ϕ_p^G. The divergence follows a power law with the exponent equal to the difference between both values of γ.

The maximum in the self-diffusion coefficient (upper-right corner of Fig. 9) is a consequence of the reentrant glass transition at high packing fractions [48,62–64]. A weak short-range attraction at first destabilizes the cage and thus the glass transition moves to higher particle concentration initially, as the polymer fraction is increased. At constant colloid concentration the diffusion thus first speeds up with increasing ϕ_p, until for intermediate attraction strengths the gel line is approached, where the opposite trend then dominates. At $\phi_c = 0.40$, the glass transition is rather far removed and thus has little effect, but the increase in D is still measurable and the diffusion coefficient can be used as a measure of the distance to the closest transition. The maximum thus indicates the reentrant shape of the nonergodicity line.

The wave-vector dependence of the time scale τ_q can also be compared with theoretical predictions. At low q, the time scale is expected to behave as q^{-2}, corresponding to a diffusive process over large distances. Yet, because the simulated scattering functions exhibit nonexponential relaxation even for the smallest wave vectors, this simple theoretical scenario is not expected to appear in our case. At intermediate wave vectors, where the Kohlrausch exponent becomes comparable to the von Schweidler one, the theory predicts a decrease as $q^{-1/b}$, whereas at even higher q the distances involved are dominated by the microscopic dynamics, and corrections to this behavior are expected [65]. The inset to Fig. 10 shows τ_q for different states close to the gel transition. In order to make clear common properties the curves have been scaled vertically to collapse (main figure).

It can be seen in this figure that the behavior of τ_q at low wave vectors (below $q = 10$), indeed shows a q^{-2} behavior, which however is not the one explained by MCT. At higher q, another power-law trend is observed, with a higher exponent: $q^{-3.3}$. The crossover from the low-q behavior to the high-q one compares nicely with the wave vector where the Kohlraush exponent becomes equal to the von Schweidler one (Fig. 7). The exponent of the high-q region yields $b = 0.30$, lower than the value obtained from the analysis in Fig. 5. However, this value is quite close to the measured von Schweidler value and much smaller than the HSS one. Deviations from this power-law behavior are observed at high q for the lowest ϕ_p presented in the figure. These deviations are caused by the microscopic dynamics, as they occur when τ_q is lower than a certain value, regardless the polymer fraction. This value, presented in the inset as a horizontal line, is $t_0 \sim 0.6$, which agrees with the time one would estimate from the correlators in Fig. 5.

C. Mean squared displacement

We turn now our attention to the MSD curves, which were partially analyzed to obtain the diffusion coefficients presented in Fig. 9. We are only interested in the slowing down close to the gel transition and thus we do not show the MSD for low polymer fractions, where the attraction speeds up the dynamics and increases the diffusivity (see Fig. 9 and Refs. [48,62,64]). The MSD, after a short initial regime of free flight $\delta r^2 \propto t^2$, slows down because of the particle interactions and takes longer and longer to reach the long-time regime diffusive, where $\delta r^2 = 6D_s t$. An important feature that can be obtained from the MSD of the particles in the system is the localization length, where the particle interactions hinder particle motion most strongly and, in the idealized

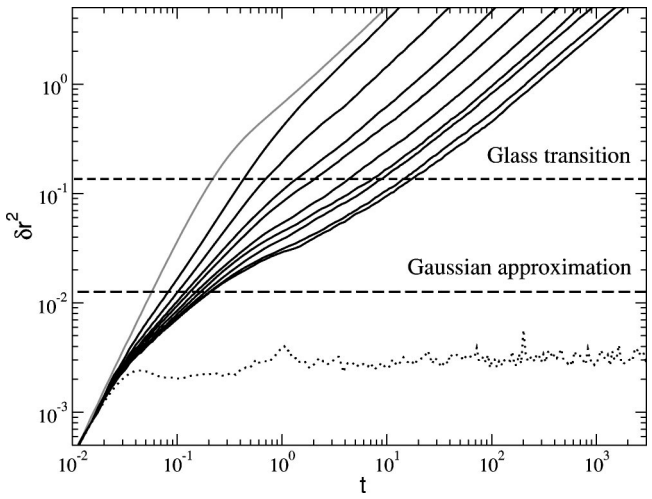

FIG. 11. Mean squared displacement of the particles as the gel transition is approached. Black curves from left to right: $\phi_p = 0.30, 0.325, 0.35, 0.375, 0.39, 0.40, 0.41, 0.415, 0.42, 0.425$. Grey curve: $\phi_p = 0$. The dashed horizontal lines indicate the localization length corresponding to the glass transition (short dash) in the HSS and the estimate from Fig. 6 (long dash). Dotted curve: mean squared displacement for a single particle in a frozen environment at $\phi_p = 0.425$.

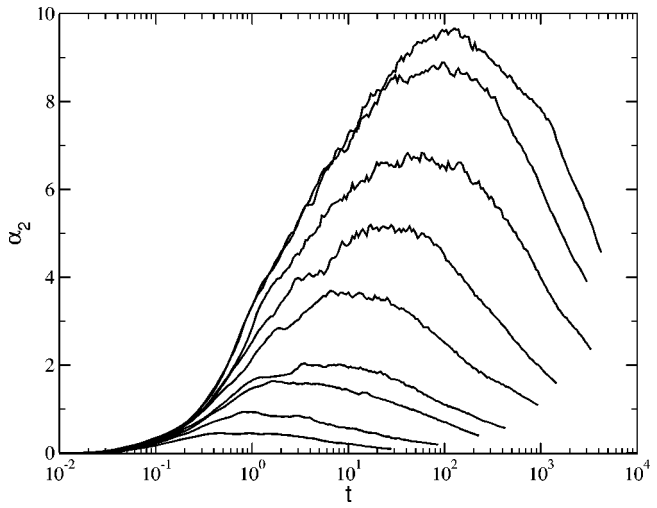

FIG. 12. Non-Gaussian parameter α_2 as a function of time for states approaching the gel transition at the same states as Fig. 11. The maximum increases with increasing ϕ_p.

glass state, arrest it. It can be compared with the estimate using the Gaussian approximation (see Fig. 6). In Fig. 11 we present the MSD for increasing polymer volume fractions. As the gel transition is approached, the localization length shows up as an indication of a plateau, signaling the bond formation. As discussed above, r_l is much shorter than in the HSS glass transition (upper dashed line in Fig. 11), because of the driving mechanism [48].

The lower dashed line in this figure is the localization length, as estimated from the nonergodicity parameter using the Gaussian approximation ($r_l^2 = 0.0126$). Although a clear plateau has not fully developed in our curves, its height seems to be above that estimate by a factor ~ 1.5–2. Since the Gaussian approximation works very well in the case of the HSS, this suggests big non-Gaussian corrections at the gel transition. Before testing the Gaussian approximation, we stress that the localization length gives a typical size of the mesh of bonds formed between neighboring particles, and that the slow structural units are continuously and cooperatively rearranging. In order to test this idea about a correlated region that cooperatively rearranges with and around each particle, a single mobile particle is considered in a fixed environment. A well equilibrated system with $\phi_p = 0.425$ is frozen, and only one particle is allowed to move. This mobile particle now explores a *frozen* environment, providing the *structural* size of the region it is confined to. The mean squared displacement so obtained is given in Fig. 11 (dotted line). Some particles (1.6%) were able to break their bonds and diffuse freely in the frozen environment. For the particles that stay localized, it can be observed that the length of the frozen bonds is much smaller than the localization length. This fact demonstrates that the structure of bonds, such as the repulsive cage at the glass transition in the HSS or LJS, is dynamic and constantly rearranges cooperatively. This collective restructuring of the system fluidizes it and restores ergodicity, which cannot occur in the frozen system, where the particles are not able to diffuse even at very long times.

We turn now back to the Gaussian approximation and its accuracy. Usually, this is tested by measuring the non-Gaussian parameter defined as

$$\alpha_2 = \frac{3\langle r^4(t)\rangle}{5\langle r^2(t)\rangle^2} - 1, \tag{12}$$

where the averages imply ensemble averaging. This parameter measures the deviation of the probability density function for the single-particle motion from the Gaussian behavior, and vanishes for diffusive motion. Special care must be taken when performing the ensemble averages in polydisperse systems, as pointed out in Ref. [66]. The non-Gaussian parameter must be calculated for every particle (the averages in the definition above thus implying time-origin averaging only), and particle averaging is taken on the values of α_2 (so long as long enough time intervals are studied, each particle will sample the distribution relevant to its own size in an ergodic fashion). The non-Gaussian parameters for states with increasing ϕ_p are presented as a function of time in Fig. 12. At short times α_2 tends to zero, since the system shows Gaussian behavior during its unhindered ballistic regime. At long times, when the particles break free from their bonds and hydrodynamic diffusion holds, α_2 again goes back towards zero. At intermediate times, corresponding to the plateaus in both the correlation function and the mean squared displacement, α_2 grows, since the single-particle motion hindered by bonding is not Brownian. As a result, α_2 shows a maximum, whose height and position grow in time, because the particles take longer and longer to break free and start diffusing.

The behavior of the simulated α_2 obeys the general expectations [36,37,39], but important differences are observed in comparison with the results for the HSS or LJS. Whereas

in those cases the height of the maximum for similar (or even higher) α-relaxation times is around 2, at the gel transition much higher values are measured. Another interesting difference is the failure of the short-time scaling, observed both in the HSS and LJS. Both effects can be rationalized considering that the cage is indeed a network of bonds in the case of a gel, rather than being a cavity. The strength of these bonds is given by the intensity of the interaction and, thus, it is modified for different states, disabling the short-time collapse. Because the bonds are short ranged, they affect the particle motion from very short times onward, so that the particles feel the hindrance much longer in the gel case.

It can be concluded that the non-Gaussian corrections are very important in the gel transition. Therefore, the localization length estimated from the nonergodicity parameter may be inaccurate, as discussed above. However, it still provides an indication of how small the localization length is. A better indication of r_l can be obtained within the Gaussian approximation if only low wave vectors are used in fitting expression (9). The fitted curve is presented in Fig. 6 by the dashed line, where only the three lowest q's are fitted. The estimated f_q^s deviates from the data at higher wave vectors, showing high non-Gaussian corrections. The localization length is higher than the previous value: $r_l^2=0.0162$. Thus, this fitting provides data more consistent with the MSD curves and the non-Gaussian parameter.

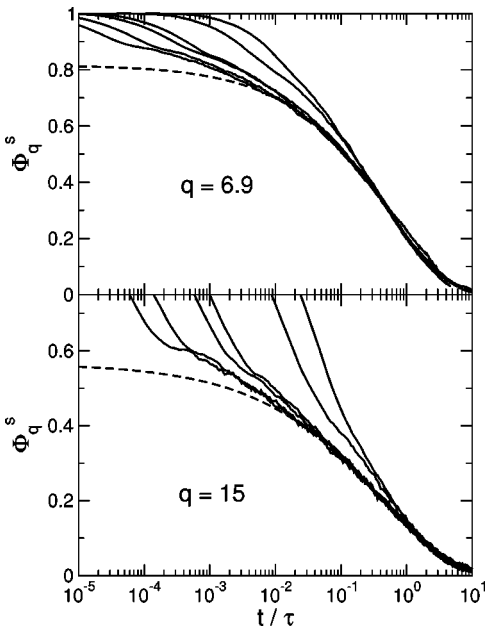

FIG. 13. Correlation functions for $\phi_c=0.50$ and different polymer concentrations. From left to right: $\phi_p=0.35,0.36,0.375,0.38,0.385,0.39$. Two wave vectors are studied, as labeled in the figures. The dashed lines represent the KWW fittings to the $\phi_c=0.40$ correlation functions.

D. Higher colloid volume fraction

We move now to a higher colloid volume fraction: $\phi_c=0.50$. These results are presented to supplement the findings at the lower packing fraction and test for the prediction of stronger stretching closer to the higher-order singularity. As indicated in the theoretical section, MCT predicts a higher-order singularity in the vicinity of the junction of the gel and glass lines, i.e., at high polymer and colloid densities. In this particular system we found clear indications of this singularity in simulations at $\phi_c=0.55$ and $\phi_p=0.375$ [40]. The isochore under study now, $\phi_c=0.50$, could be close enough to the higher-order singularity to show some effects.

In Fig. 13 we present the correlation functions for increasing polymer fractions at the same wave vectors as Fig. 4, rescaled to collapse in the long-time decay. It is interesting to note that the polymer concentrations studied in this case are lower than those studied at the lower colloid volume fraction. In accordance with experiments and theory, this indicates that the gel transition takes place at lower polymer fractions the higher the colloid concentration.

In Fig. 13, it can be observed that the correlators do not collapse over the whole α decay, but only in the end. These deviations are expected because of the higher-order singularity, which is at higher densities. However, we stress that although this singularity has clear effects on the correlation functions, they do not show so clear signatures as that of the $\phi_c=0.55$ isochore [40]. At this high concentration, a logarithmic decay was observed, with a wave vector-dependent extension.

Because these corrections affect the early α decay, analyzing the correlation functions is difficult. Furthermore, the plateau is not observed and the von Schweidler analysis is thus extremely difficult. In order to analyze the self-intermediate scattering function, we compare the stretching of the curves at $\phi_c=0.40$ and $\phi_c=0.50$; in Fig. 13 the α decay master function of the $\phi_c=0.40$ state, as parametrized by the KWW fitting, is included. It can be seen that this curve can be rescaled to collapse onto the α decay of the correlators at $\phi_c=0.50$ for both wave vectors at long times. This indicates not only that the von Schweidler exponent is very similar in both cases, but also points out the effect of the high-order singularity. According to MCT, b should decrease as the singularity is approached, but this behavior is not observed in our case. Comparison of the α decays by fitting the KWW stretched exponential to the master function is troublesome, since only the late decay is obtained unambiguously.

The similarity of both α decays was used in the von Schweidler analysis of the correlation function, and only the nonergodicity parameter and amplitudes were fitted. Since the upper part of the decay is known to be affected by the higher-order singularity close by, that part must be discarded in the fittings. The correlation functions and fittings are presented in Fig. 14 for the state $\phi_c=0.50$ and $\phi_p=0.39$, for the same wave vectors as in Fig. 5. The main conclusion is that the late α decay at all wave vectors can be correctly described by the von Schweidler decay, with the same exponent as the state at $\phi_c=0.40$. The nonergodicity parameters obtained from the fitting are slightly lower than those of $\phi_c=0.40$, but similar within the error bars. According to MCT, f_q^s decreases when approaching the glass part of the nonergodicity line (signaling an increase in the localization length). Our result is thus consistent with this prediction.

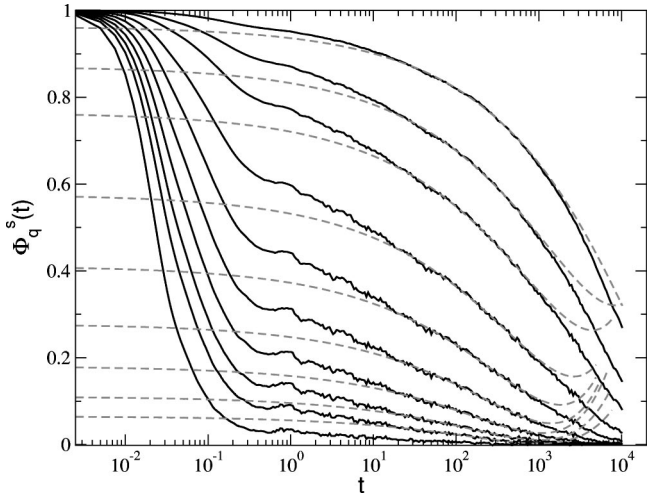

FIG. 14. Intermediate scattering function (self-part) Φ_q^s for the same wave vectors as in Fig. 5 for $\phi_c=0.50$ and $\phi_p=0.39$. The dashed lines are fittings from Eq. (3) up to second order, with the same von Schweidler exponent as $\phi_c=0.40$.

With these values of the nonergodicity parameter, one can define also the wave-vector-dependent time scale τ_q as discussed above. In order to test the value of the von Schweidler exponent, using Eq. (11) we have performed a three-parameter fitting to obtain γ and ϕ_p^G. In Fig. 15, τ_q is presented as a function of $\phi_p^G-\phi_p$ for different wave vectors. The power-law fittings for two wave vectors are also plotted and the critical polymer fraction ϕ_p^G is given.

The values of γ obtained from this analysis for different wave vectors range from $\gamma=3.37$ to $\gamma=3.82$; the mean value being $\gamma=3.70$. This value of γ implies a smaller von Schweidler exponent $b=0.33$, in disagreement with our previous estimate, but backing the MCT prediction. Using the same value of ϕ_p^G, the vanishing of the self-diffusion coefficient D_s can be analyzed and is presented in the inset to this figure. A power law is observed in this case, with an exponent $\gamma=1.92$, which, again in contradiction to MCT, leaves us with a big difference between the two values of γ.

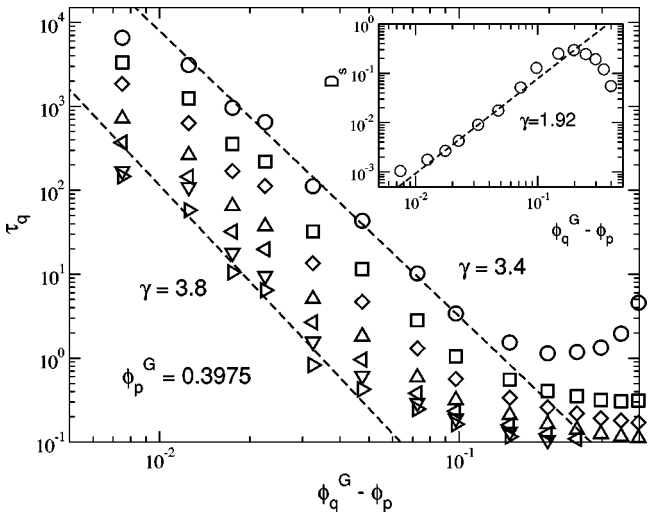

FIG. 15. Wave-vector-dependent time scale τ_q vs $\phi_p^G-\phi_p$ for different wave vectors; symbols from top to botton correspond to $q=3.9,6.9,9.9,15,20,25,30$. The lines are power-law fittings to $q=3.9$ and $q=30$. ϕ_p^G and γ were fitted.

The diffusion coefficients in the inset of Fig. 15 again indicate the reentrant glass transition. They describe a maximum, more pronounced than that observed in Fig. 9, because the glass line is closer to the $\phi_c=0.50$ isochore. The minimum in τ_q, which is observed only for $q=3.9$, in an equivalent way indicates the shape of the nonergodicity transition line. At higher wave vectors, the glass transition causes very low f_q^s and the time scales merge with the microscopic transient and thus this feature is suppressed.

The wave vector dependence of τ_q can also be studied, as done for the lower concentration, yielding another estimate of *b*. In this case, a similar plot as Fig. 10 is obtained, where the low-*q* region is compatible with a q^{-2} behavior, and a higher exponent at higher *q*, yielding a value of $b=0.38$. This value is in agreement with the nice comparison between the $\phi_c=0.40$ and $\phi_c=0.50$ isochores, but not with γ or the MCT prediction. We may then conclude that an analysis of this state is extremely difficult, but our indications state that the von Schweidler exponent is similar for both packing fractions, but probably slightly lower in the higher concentration.

Finally, we would like to point out that the non-Gaussian parameter at this packing fraction shows a behavior similar to that shown in Fig. 12, i.e., the peak is as high, and no short-time scaling is observed.

V. CONCLUSIONS

In this paper, by means of simulations, we have tested the universal predictions of MCT for gelation in colloidal systems, viewed as an attraction-driven glass transition. The self-parts of the intermediate scattering function for states close to this transition have been analyzed and the results were compared with the theoretical predictions. For the $\phi_c=0.40$ isochore, which is far enough from the high-order singularity, the correlation functions can be α scaled. The time scale of the α decay was shown to obey a power-law divergence, with an exponent γ related to the von Schweidler exponent, obtained from the early α decay. Both features are predicted by MCT for all nonergodicity transitions. Also, the wave vector analysis of the time scale follows the behaviors predicted by MCT, with a small difference in the value of the von Schweidler exponent.

The wave-vector analysis of the correlation functions depends on details of the interaction potential, and thus provides information about the mechanism, leading to the transition. In our case, it establishes that the gel transition is driven by a short-range mechanism, namely, bond formation, as observed in the pair distribution function. Additionally, it has been shown that the KWW stretched exponential can account for the α decay of the correlation functions, as in other nonergodicity transitions.

We have also tested the Gaussian approximation, which works very well for the HSS. The non-Gaussian parameter α_2 establishes that this approximation is much worse in the case of the gel transition than for the glass transition. It was

also tested when comparing the estimated localization length from the nonergodicity parameter with the MSD of the particles. The diffusion coefficient has been also studied. It tends to zero as the transition is approached following a power law, with an exponent much lower than γ, in accordance with simulations of glass transitions in other systems, but in disagreement with MCT, where both exponents are equal.

Finally, when the colloid concentration is increased, the system shows signatures of the high-order singularity nearby and little can be discussed about the exponents b or γ. However, only slight changes in the numbers are expected, since the qualitative behavior is reproduced, except for the α scaling. Also, the diffusion coefficient follows a power law with a different exponent and the non-Gaussian parameter reaches values similar to the $\phi_c = 0.40$ case.

Therefore, our main conclusion is that MCT accounts for most features of the simulated systems on approach to the gel transition, but the discrepancies already found in other nonergodicity transitions (such as the repulsion-driven glass transition in hard-sphere systems) are also obtained here.

ACKNOWLEDGMENTS

The authors thank W. Kob and R. Sear for useful discussion. A.M.P. acknowledges the financial support by the CICYT (Project No. MAT2000-1550-CO3-02). M.F. was supported by the DFG under Grant No. Fu 309/3.

[1] *Soft and Fragile Matter, Nonequilibrium Dynamics, Metastability and Flow,* edited by M. E. Cates and M. R. Evans (Institute of Physics, Bristol, 2000).
[2] W.C.K. Poon, L. Starrs, S.P. Meeker, A. Moussaid, R.M.L. Evans, P.N.P. Pusey, and M.M. Robins, Faraday Discuss. **112**, 143 (1999).
[3] A. Imhof and J.K.G. Dhont, Phys. Rev. Lett. **75**, 1662 (1995).
[4] L. Cipelletti, S. Manley, R.C. Ball, and D.A. Weitz, Phys. Rev. Lett. **84**, 2275 (2000).
[5] M. Muschol and F. Rosenberger, J. Chem. Phys. **107**, 1953 (1997).
[6] M. Carpineti and M. Giglio, Phys. Rev. Lett. **68**, 3327 (1992).
[7] W.C.K. Poon and M.D. Haw, Adv. Colloid Interface Sci. **73**, 71 (1997).
[8] P.N. Segré, V. Prasad, A.B. Schofield, and D.A. Weitz, Phys. Rev. Lett. **86**, 6042 (2001).
[9] K. Kroy *et al.* (unpublished).
[10] J. Bergenholtz and M. Fuchs, Phys. Rev. E **59**, 5706 (1999).
[11] J. Bergenholtz and M. Fuchs, J. Phys.: Condens. Matter **11**, 10171 (1999).
[12] J. Bergenholtz, M. Fuchs, and Th. Voigtmann, J. Phys.: Condens. Matter **12**, 6575 (2000).
[13] W. van Megen, T.C. Mortensen, S.R. Williams, and J. Müller, Phys. Rev. E **58**, 6073 (1998).
[14] S.R. Williams and W. van Megen, Phys. Rev. E **64**, 041502 (2002).
[15] C. Beck, W. Härtl, and R. Hempelmann, J. Chem. Phys. **111**, 8209 (1999).
[16] E. Bartsch, T. Eckert, C. Pies, and H. Sillescu, J. Non-Cryst. Solids **307**, 802 (2002).
[17] W. Götze and R. Haussmann, Z. Phys. B: Condens. Matter **72**, 403 (1988).
[18] W. Götze and L. Sjögren, J. Phys.: Condens. Matter **1**, 4203 (1989).
[19] W. Gotze and M. Sperl, Phys. Rev. E **66**, 011405 (2002).
[20] L. Fabbian, W. Gotze, F. Sciortino, P. Tartaglia, and F. Thierry, Phys. Rev. E **59**, R1347 (1999); **60**, 2430 (1999).
[21] K. Dawson, G. Foffi, M. Fuchs, W. Götze, F. Sciortino, M. Sperl, P. Tartaglia, Th. Voigtmann, and E. Zaccarelli, Phys. Rev. E **63**, 011401 (2001).
[22] W. Kob and H.C. Andersen, Phys. Rev. E **51**, 4626 (1995).
[23] W. Kob and H.C. Andersen, Phys. Rev. E **52**, 4134 (1995).
[24] T. Gleim, W. Kob, and K. Binder, Phys. Rev. Lett. **81**, 4404 (1998).
[25] T. Gleim and W. Kob, Eur. Phys. J. B **13**, 83 (2000).
[26] F. Sciortino, P. Gallo, P. Tartaglia, and S.H. Chen, Phys. Rev. E **54**, 6331 (1996).
[27] F. Sciortino, L. Fabbian, S.H. Chen, and P. Tartaglia, Phys. Rev. E **56**, 5397 (1997).
[28] C. Bennemann, W. Paul, K. Binder, and B. Dünweg, Phys. Rev. E **57**, 843 (1998).
[29] C. Bennemann, J. Baschnagel, and W. Paul, Eur. Phys. J. B **10**, 323 (1999).
[30] C. Bennemann, J. Baschnagel, W. Paul, and K. Binder, Comput. Theor. Polym. Sci. **9**, 217 (1999).
[31] M. Aichele and J. Baschnagel, Eur. Phys. J. E **5**, 229 (2001); **5**, 245 (2001).
[32] D. Caprion and H.R. Schober, Phys. Rev. B **62**, 3709 (2000).
[33] F. Sciortino and W. Kob, Phys. Rev. Lett. **86**, 648 (2001).
[34] J. Horbach and W. Kob, Phys. Rev. E, **64**, 041503 (2001).
[35] M. Nauroth and W. Kob, Phys. Rev. E **55**, 657 (1997).
[36] C. Donati, S.C. Glotzer, and P.H. Poole, Phys. Rev. Lett. **82**, 5064 (1999).
[37] C. Donati, S.C. Glotzer, P.H. Poole, W. Kob, and S.J. Plimpton, Phys. Rev. E **60**, 3107 (1999).
[38] B. Doliwa and A. Heuer, Phys. Rev. Lett. **80**, 4915 (1998).
[39] B. Doliwa and A. Heuer, Phys. Rev. E **61**, 6898 (2000).
[40] A.M. Puertas, M. Fuchs, and M.E. Cates, Phys. Rev. Lett. **88**, 098301 (2002).
[41] M. Fuchs, I. Hofacker, and A. Latz, Phys. Rev. A **45**, 898 (1992).
[42] M. Fuchs, W. Götze, and M.R. Mayr, Phys. Rev. E **58**, 3384 (1998).
[43] S. Asakura and F. Oosawa, J. Chem. Phys. **22**, 1255 (1954).
[44] A.P. Gast, C.K. Hall, and W.B. Russel, J. Colloid Interface Sci. **96**, 251 (1983).
[45] A.P. Gast, W.B. Russel, and C.K. Hall, J. Colloid Interface Sci. **109**, 161 (1986).
[46] M. Dijkstra, R. van Roij, and R. Evans, Phys. Rev. Lett. **81**, 2268 (1998).
[47] M. Dijkstra, R. van Roij, and R. Evans, Phys. Rev. E **59**, 5744 (1999).

[48] E. Zaccarelli, G. Foffi, K.A. Dawson, S.V. Buldyrev, F. Sciortino, and P. Tartaglia, Phys. Rev. E **66**, 041402 (2002).
[49] W. Götze in *Liquids, Freezing and Glass Transition*, edited by J.P. Hansen, D. Levesque, and J. Zinn-Justin (North-Holland, Amsterdam, 1991).
[50] W. Götze and L. Sjögren, Rep. Prog. Phys. **55**, 241 (1992).
[51] J.P. Hansen and I.R. McDonald, *Theory of Simple Liquids* (Academic, London, 1986).
[52] J.R. Melrose, Europhys. Lett. **19**, 51 (1992).
[53] J.M. Méndez-Alcaraz and R. Klein, Phys. Rev. E **61**, 4095 (2000).
[54] P.J. Steinhardt, D.R. Nelson, and M. Ronchetti, Phys. Rev. B **28**, 784 (1983).
[55] R.P. ten Wolde, M.J. Ruiz-Montero, and D. Frenkel, J. Chem. Phys. **104**, 9932 (1996).
[56] R.P. Sear and W.M. Gelbart, J. Chem. Phys. **110**, 4582 (1999).
[57] G. Foffi, G.D. McCullagh, A. Lawlor, E. Zaccarelli, K.A. Dawson, F. Sciortino, P. Tartaglia, D. Pini, and G. Stell, Phys. Rev. E **65**, 031407 (2002).
[58] M. Fuchs, J. Non-Cryst. Solids **172-174**, 241 (1991).
[59] A. Tölle, J. Wuttke, W. Schober, O.G. Randl, and F. Fujara, Eur. Phys. J. B **5**, 231 (1998).
[60] F.W. Starr, S. Harrington, F. Sciortino, and H.E. Stanley, Phys. Rev. Lett. **82**, 3629 (1999).
[61] This state was carefully checked for aging or out-of-equilibrium effects; but within our tests, it is fully equilibrated.
[62] K.N. Pham, A.M. Puertas, J. Bergenholtz, S.U. Egelhaaf, A. Moussaid, P.N. Pusey, A.B. Schofield, M.E. Cates, M. Fuchs, and W.C.K. Poon, Science **296**, 104 (2002).
[63] G. Foffi, K.A. Dawson, S.V. Buldyrev, F. Sciortino, E. Zaccarelli, and P. Tartaglia, Phys. Rev. E **65**, 050802 (2002).
[64] T. Eckert and E. Bartsch, Phys. Rev. Lett. **89**, 125701 (2002).
[65] M. Fuchs and M.R. Mayr, Phys. Rev. E **60**, 5742 (1999).
[66] B. Doliwa and A. Heuer, J. Phys.: Condens. Matter **11**, A277 (1999).